Multidimensional Polypyrrole/Iron Oxyhydroxide Hybrid Nanoparticles for Chemical Nerve Gas Agent Sensing Application

Jun Seop Lee, Dong Hoon Shin, Jaemoon Jun, and Jyongsik Jang*

World Class University (WCU) Program of Chemical Convergence for Energy and Environment (C2E2), School of Chemical and Biological Engineering, College of Engineering, Seoul National University (SNU), 599 Gwanangno, Gwanak-gu, Seoul, 151-742 Korea

ABSTRACT Multidimensional FeOOH nanoneedle-decorated hybrid polypyrrole nanoparticles (PFFs) were fabricated using dual-nozzle electrospray and heat stirring process. To decorate metal oxide nanoneedles on the polypyrrole (PPy) surface, metal oxide particle-decorated PPys (E_PPy) were fabricated as starting materials. The E_PPy particles were prepared by dual-nozzle electrospray because ferric ions (Fe^{3+}) dispersed on the surface reacted with hydroxide (OH^-) ions in the collector solution without aggregation of each particles. Multidimensional hybrid PFFs with maximized surface area were then formed by heat stirring reaction in the aqueous metal precursor contained solutions. The decoration morphology of the metal oxide nanoneedles could be controlled by precursor concentration in the aqueous solution. These multidimensional hybrid PPFs were applied to nerve gas agent (DMMP) chemical sensor at room temperature with excellent sensitivity. The minimum detectable level (MDL) of PFFs was as low as 0.1 ppb, which is higher than that for a chemical sensor based on hybrid materials. This is because the metal oxide nanoneedles increase surface area and affinity to DMMP vapor.

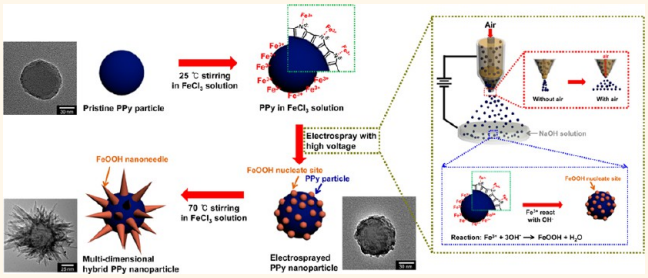

KEYWORDS: electrospray · polypyrrole · room temperature gas sensing · metal nanoneedle decoration · DMMP gas

Since the discovery of poly(acetylene) in 1977, various types of conducting polymers have been discovered and investigated for numerous applications because of the versatile nature of these polymers originate from polyconjugated chains consisting of alternating single and double bonds.[1−10] Among various applications, conducting polymers have been used as sensors, due to their inherent electronic, optic, and mechanical transduction mechanism.[11−18] To enhance sensitivity, considerable effort has focused on the fabrication of nanometer-scale conducting polymer materials; the beneficial characteristics of these materials include their small dimensions, high surface-to-volume ratio, and amplified sensitivity for sensor-transducer applications.[19−23] Among various morphology of conducting polymer nanostructures, nanoparticles offer the advantages of (1) small-diameter particles for device fabrication, (2) facile fabrication steps and uniform size, and (3) uniform deposition for sensor electrode production, without particle aggregation.[24−29]

The development of chemical warfare has produced weapons used to terrorize people in times of war and peace, for example, the gas attack on the Tokyo subway in 1995, in particular, odorless, colorless, chemical warfare agents (CWAs), such as Sarin, Soman, and Tabun, composed of organophosphorous compounds that disrupt the mechanism by which nerves transfer messages to organs in the body.[30,31] Therefore, these toxic chemicals have motivated intensive research in the development of sensitive, selective, portable gas sensors. However, there are several limitations to detect these gases in air owing to their dangerous and fatal impact to humans. Thus, instead of toxic nerve chemicals, simulants for nerve gases that have similar chemical structure and the same sensing mechanism are used to detect

* Address correspondence to jsjang@plaza.snu.ac.kr.

Received for review August 20, 2013 and accepted October 23, 2013.

Published online October 23, 2013
10.1021/nn404353w

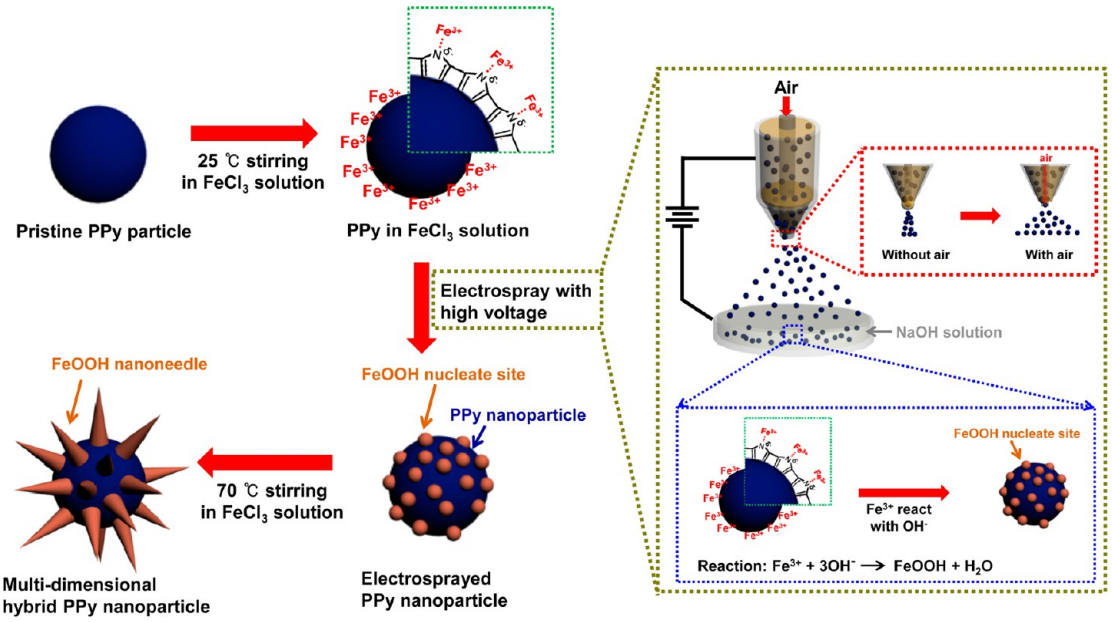

Figure 1. Illustrative diagram of the sequential fabrication steps for multidimensional hybrid polypyrrole nanoparticles (green inset: schematic illustration of the formation of FeOOH nucleate site by using dual-nozzle electrospray method with compressed air blowing (red inset: comparison of electrosprayed particles by control compressed air blowing)).

in air. Among chemical nerve gas agents, dimethyl methylphosphonate (DMMP) has a similar structure to Sarin, is used to detect for simulant for Sarin, and also requires a method for its detection in air.

Recently, several scientific approaches have been devised to detect these nerve agents, such as colorimetric analysis, mass spectroscopy, enzymatic assay, gas chromatography, molecular imprinting, and photoacoustic spectroscopy.[32−36] Although all of these methods have advantages, critical limitations remain, including low sensitivity, slow response time, high cost, and limited portability, particularly, operational complexity for colorimetric analysis and temperature-dependent for enzymatic assay. On the other hand, interdigitated array (IDA) based chemiresistive sensors have several strengths to apply chemical nerve agent sensing. First, it shows high sensitivity and fast response time than other detection approaches in air on account of fast signal transfers from transducer materials to the electrode. Another strength is the simple measurement with real-time changing resistance of the electrode without additional measurement steps during target analyte detection. The cycle ability is the other strength of the IDA sensing device without any defect during repeated target chemical sensing.

Herein, we present a new simple strategy for fabricating multidimensional hybrid polypyrrole (PPy) nanoparticles, decorated vertically with metal oxide (FeOOH) nanoneedles. A dual-nozzle electrospray technique is described that can positively charge the particle surface to form FeOOH nucleate sites for nanoneedle growth during a heat reaction process. Particle aggregation was prevented by compressed air flow through the inner part of the dual-nozzle. The multidimensional hybrid PPy nanoparticles were utilized as a transistor for a nerve gas agent (DMMP) chemical sensor. The sensing response of this sensor was ultrasensitive and reversible due to the multidimensional structure of the sensor transducer, which maximized the surface area of the particles. The minimum detectable level (MDL) was as low as 0.1 ppb compared with higher than that of a chemical sensor based on metal oxide hybrid materials.[37,38] To our knowledge, no reports have described the manufacture of multidimensional conducting polymer−metal oxide hybrid composites using the dual-nozzle electrospray technique.

RESULTS AND DISCUSSION

Fabrication of Multidimensional Hybrid PPy Particles. Figure 1 illustrates the overall procedure for the fabrication of multidimensional hybrid PPy nanoparticles, based on the dual-nozzle electrospray method. First, 60 nm diameter PPy particles were prepared using a monodisperse method, described in our previous work (Figure S1).[39] PPy nanoparticles were stirred in an $FeCl_3$ aqueous solution at room temperature to induce covalent bonding between the Fe^{3+} ions and the partial negative charge of the N atom in the pyrrole structure. The mixed PPy solutions were electrosprayed by the outer part of the dual-nozzle, while compressed air flowed through the inner nozzle. The electrosprayed PPy (E_PPy) particles were collected by a Petri dish collector, under a continuous high voltage. During the electrospray process, FeOOH particle formation on the PPy surfaces was facilitated by several factors (green inset of Figure 1). The high positive voltage applied allowed uniform dispersion of Fe^{3+} ions on the PPy surfaces, resulting in

positively charged electrosprayed PPy nanoparticles. Additionally, the mechanical force, provided by the compressed air flow through the inner part of the dual-nozzle, broke up the mixed PPy solution drops into small nanosized droplets; this reduced the likelihood of particle aggregation (Figure 2a,b). Finally, the Fe^{3+} ions reacted with the hydroxide ions in the collector; thus, when the electrosprayed particles were collected in a solution containing NaOH, the Fe^{3+} ions reacted with the hydroxide ions to form FeOOH particles, as described by the following reaction:[40,41]

$$Fe^{3+} + 3OH^- \rightarrow FeOOH + H_2O \quad (1)$$

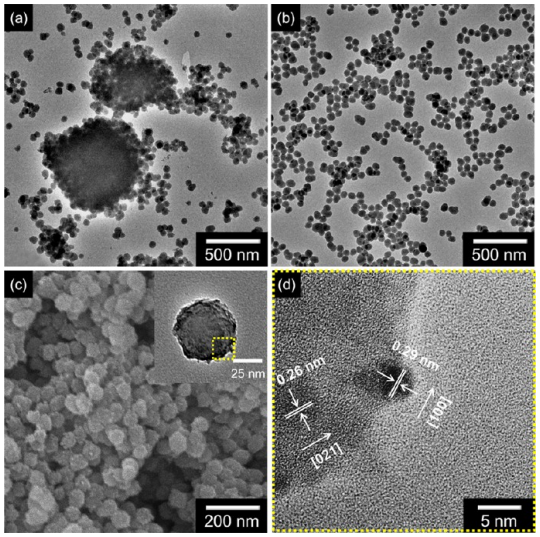

Figure 2. TEM images of E_PPy nanoparticles (a) without compressed air and (b) with compressed air during electrospray process. (c) SEM and TEM (inset) image of E_PPy nanoparticles after reacted with hydroxide (OH^-) ions. (d) HR-TEM image of FeOOH nucleate sites on the E_PPy nanoparticle.

Figure 2c shows the E_PPy nanoparticles decorated with about 3 nm diameter metal particles on their surface. High-resolution transmission electron microscopy (HR-TEM) images indicated an interplanar spacing between the metal particles of 0.29 and 0.26 nm for the (100) and (021) planes, respectively, corresponding to the α-FeOOH lattice structure (Figure 2d).

The E_PPy nanoparticles were stirred in an $FeCl_3$ aqueous solution at 70 °C for 4 h to induce growth of FeOOH needles on the surface. The Fe^{3+} ions in the solution were converted into FeOOH needles at the decorated FeOOH particle sites (*i.e.*, the FeOOH particles acted as nucleate sites during this process). The morphology and needle density were controlled by the concentration of the $FeCl_3$ aqueous solution, which varied from 0.5 to 10 wt %. This resulted in FeOOH-nanoneedle-decorated PPy nanoparticles (denoted as PFFs), with various needle morphologies on the surface.

The nanostructures of the hybrid PFFs had different FeOOH nanoneedle configurations. The PFFs with 0.5, 2.0, 5.0, and 10.0 wt % FeOOH precursors are denoted as PFF_0.5, PFF_2, PFF_5, and PFF_10, respectively (Figure 3). TEM and HR-TEM images show that the length and diameter of the FeOOH nanoneedles increased with the precursor concentration. At low

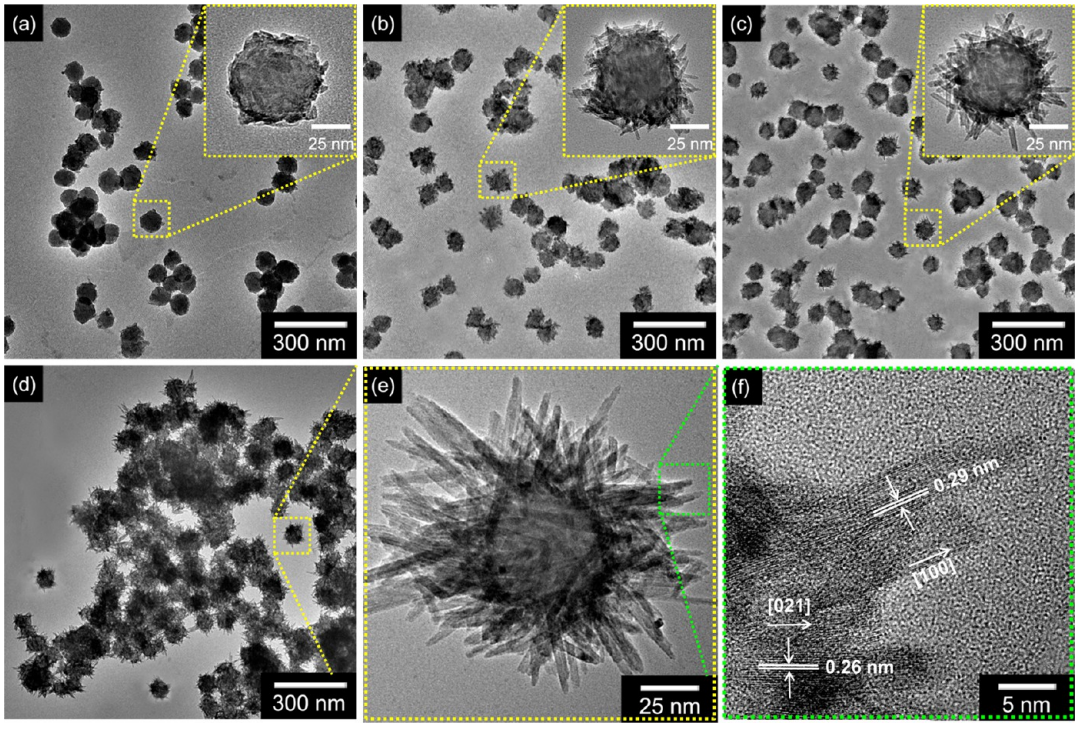

Figure 3. Low and high (inset) resolution TEM images of hybrid PFF nanoparticles with various concentration of $FeCl_3$ solutions: (a) 0.5 wt %, (b) 2.0 wt %, and (c) 5.0 wt %, and 10 wt % hybrid PFF nanoparticles with (d) low resolution TEM, (e) high resolution TEM, and (f) HR-TEM images of FeOOH nanoneedles on the PPy surface.

concentrations (0.5 wt %), the about 5 nm diameter FeOOH particles decorated the surface, instead of nanoneedles. However, the 10 wt % FeOOH precursor concentration resulted in the formation of nanoneedles, about 40 nm in length and about 10 nm in diameter. The FeOOH density also increased with precursor concentration. The HR-TEM image of FeOOH indicates an interplanar spacing of 0.29 and 0.26 nm for the (100) and (021) of α-FeOOH, respectively, and confirmed growth of pure, crystalline nanoneedles following treatment (Figure 3f).

Characterization of Multidimensional Hybrid PPy Particles. The X-ray diffraction (XRD) patterns of the particles are shown in Figure 4. The peak of the inorganic material in the E_ PPy and hybrid PFF particles can be well indexed to the α-FeOOH (JCPDS 29−713), indicating the formation of α-FeOOH nanostructures on the PPy surface. As expected, the peak intensities for the α-FeOOH nanoneedles increased due to the enhancement in the nanoneedle density, following the stirring reaction procedure. The broad diffraction peaks at 25.6 cm^{-1} were observed for all samples, indicating an identical crystalline PPy structure for all of the samples. The chemical composition of the hybrid materials was also confirmed by X-ray photoelectron spectroscopy (XPS). Figure 5a shows the complete spectra over the range of 0−1200 eV. These overview spectra revealed that C, N, O, and Fe atoms were present in the PFF_10 and E_PPy samples, whereas only C, O, and N were present in the pristine PPy nanoparticles. The N 1s peak was attributed to the N component in the pyrrole structure (pyrrolylium nitrogen component and the positively charged N atoms). The high-resolution XPS spectra for the C 1s region around 285 eV are shown in Figure 5b; this peak was deconvoluted into four components. The peak at 284.3 eV was attributed to C═C bonds, and the 285.3 eV peak corresponded to the C−C bond. The C−O and C−N groups exhibited peaks at 286.6 and 284.9 eV, respectively. The C 1s peaks for the hybrid PFF_10 and E_PPy were not shifted relative to those for the pristine PPys, confirming that the structure of the PPys remained unchanged after the formation of FeOOH nanoneedles. Figure 5c shows the O 1s band of particles deconvoluted into several components. The peak at 533.0 eV represented the C−O bonds from the PPy structure component. The peaks at 531.7 and 529.6 eV were attributed to the OH^- and O^{2-} components in the FeOOH structure. Figure 5d shows the high-resolution XPS spectra for the Fe 2p peak. Spin−orbit components $2p_{3/2}$ and $2p_{1/2}$ were observed near 708.5 and 722.2 eV, indicating that the valence state of Fe

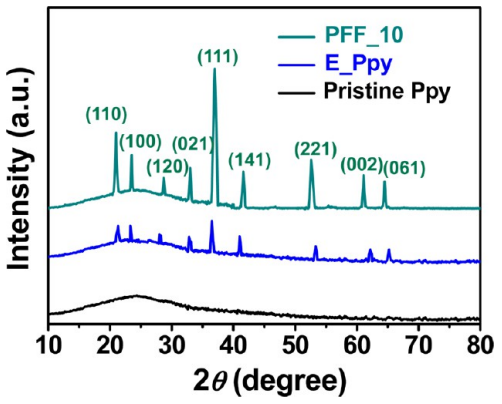

Figure 4. XRD pattern of various PPy nanoparticles (black, pristine PPy; blue, E_ PPy; green, hybrid PFFs).

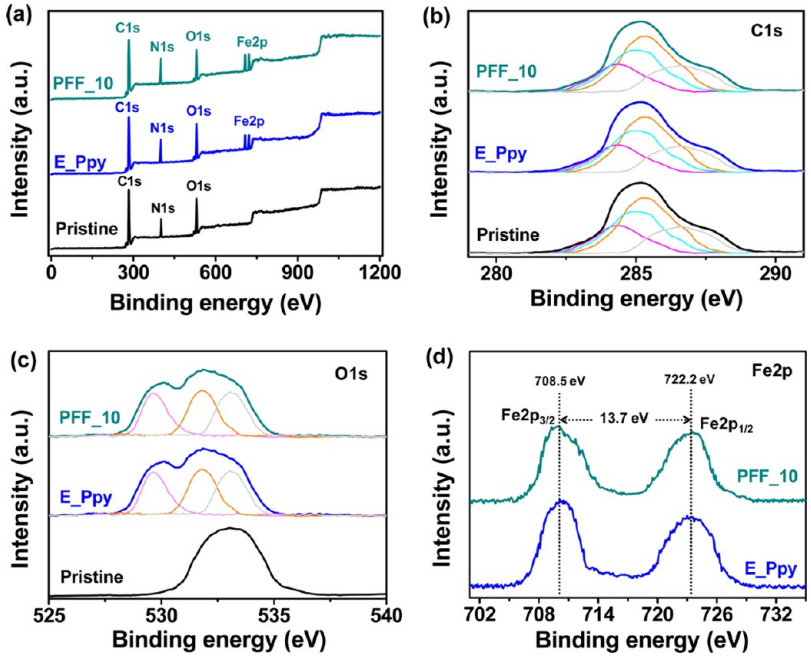

Figure 5. XPS patterns of (a) fully scanned spectra and high resolution of (b) C 1s, (c) O 1s, and (d) Fe 2p of hybrid PPy nanoparticles (black, pristine PPy; blue, E_PPy; green, PFF_10).

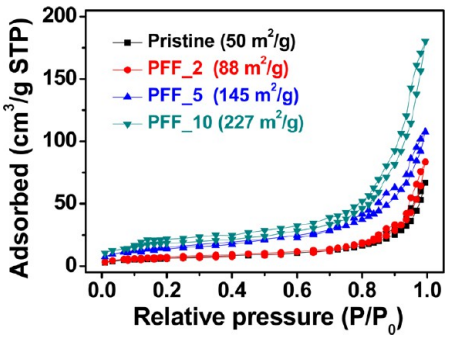

Figure 6. Nitrogen adsorption−desorption isotherm of various hybrid FeOOH/PPy nanoparticles (pristine PPy, black; PFF_2, red; PFF_5, blue; PFF_10, green).

was +3. Thus, it can be concluded that the FeOOH nanoneedles were composed of Fe(III) and O, as confirmed by XRD results. Additionally, the decoration amounts of FeOOH were quantified by TGA analysis (Figure S2).

Figure 6 shows the N_2 adsorption/desorption isotherms obtained using the Brunauer−Emmett−Teller (BET) method for the hybrid PPy nanoparticles. The surface area increased from 50 $m^2\ g^{-1}$ for pristine PPy particles to 227 $m^2\ g^{-1}$ for PFF_10. This increase in the surface area was caused by the enhancement in the nanoneedle density and size on the surface; specifically, the surface area of PFF_10 was about 4 times larger than that of the pristine PPy particle. Additionally, the surface areas of E_PPy and PFF_0.5 were 60 $m^2\ g^{-1}$ and 65 $m^2\ g^{-1}$, similar to that for pristine PPy (Figure S3). Therefore, the $FeCl_3$ solution concentration during the stirred heat reaction had a significant effect on the surface area of the hybrid PFFs, due to the enhancement of the decorated FeOOH nanoneedle size and density.

Several approaches were explored to optimize the sensor performance, that is, the conductive pathway and effective surface area. Figure 7 shows the current−voltage (*I*−*V*) curves of the hybrid PFFs; the results indicated that the hybrid nanoparticles were in good electrical contact with the sensor substrate. The transducer arrangement was thought to improve the conductive pathway, that is, to increase the DMMP detection sensitivity. The randomly stacked arrangement of PFFs prepared by the drop-casting method had a higher contact resistance than the uniform array obtained by spin-coating, due to interruption of the conductive pathway through the accumulated particle−particle assembly. Therefore, PFFs were deposited on the electrode by spin-coating to determine the sensing performance in real-time with minimized contact resistance.

Real-Time Responses of the Nerve Gas Agent (DMMP) Sensor. The uniformly dispersed PFFs on the sensor substrate rapidly detected DMMP gas at room temperature. The sensing mechanism of the hybrid PFFs is described below (Figure 8). The FeOOH surfaces adsorbed to DMMP by charge interaction and hydrogen bonding through the −OH group of FeOOH and the phosphate

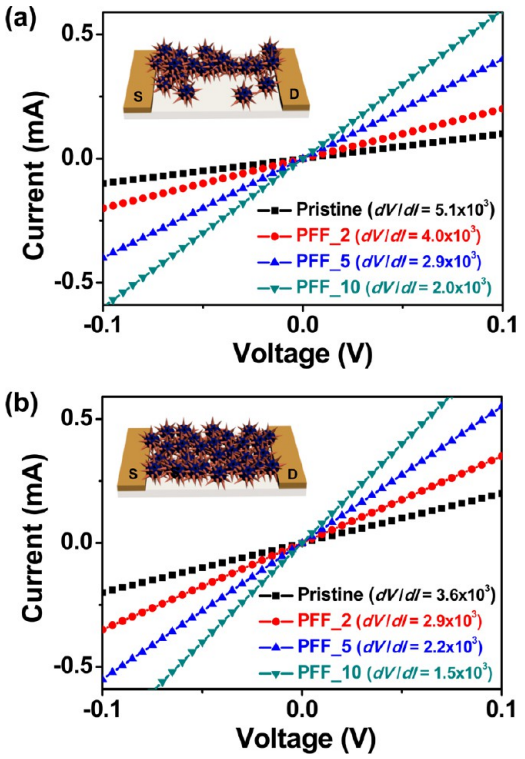

Figure 7. *I*−*V* curves of hybrid PFF nanoparticles deposited on IDA by using (a) drop-casting and (b) spin-coating method (pristine PPy, black; PFF_2, red; PFF_5, blue; PFF_10, green).

group of the DMMP structure. DMMP is a strong electron donor; thus, when the PFFs were exposed to DMMP vapors, electrons were transferred from DMMP to FeOOH; these transferred electrons flowed to the PPy structure, leading to a decrease in the number of holes in the PPy and increasing electrical resistance (because PPy acts as a p-type transducer).[42,43] The FeOOH nanoneedles performed critical effect to DMMP gas sensing in the detecting mechanism. First, it bonded to DMMP gas through not only charge interaction but also hydrogen bonding of oxygen atom in the DMMP and −OH group of FeOOH that increased functional site to DMMP gas. Second, enlarged surface area by vertically aligned on the PPy surface is also increasing DMMP sensing active site. As a result, enhancement adsorbed amount of vapors increased sensitivity to DMMP gases.

The sensing performance of the DMMP gas sensor was affected by the decorated FeOOH populations and morphologies of the surfaces. The real-time responses of various PPy nanoparticles were measured for different concentrations of DMMP gas. First, pristine PPy and E_PPy nanoparticles, without FeOOH needles, were tested (Figure 9a). In the pristine PPy case, there were no functional sites to attract DMMP gas molecules. In contrast, the E_PPy nanoparticles had numerous FeOOH nucleate sites to attract the DMMP gas to the PPy surface. However, the nucleate site is quite small in size; thus, there was little interaction with the DMMP gas. As a result, the sensitivity of the DMMP gas sensor

was absent or low for the pristine PPy and E_PPy particles. In contrast, for the hybrid PFFs, the FeOOH nanoneedle morphology and density on the PPy surfaces significantly affected the sensing performance of the DMMP gas sensor. When the hybrid PFF sensors were exposed to DMMP gas at room temperature, excellent sensitivity and rapid response/recovery times were observed. Figure 9b shows the sensor response upon sequential exposure as a function of analyte concentration. The sensitivity of hybrid PFFs increased as the size and density of FeOOH needles on the surface increased; specifically, PFF_10 was capable of detecting DMMP concentrations as low as 0.1 ppb at room temperature. Furthermore, nanoneedle size and density influence the response and recovery times to the target gas. Figure 9c shows the real-time response to DMMP of hybrid PPy particles. The response of the E_PPy nanoparticles was 2.0 s; the hybrid PFF sensor with PFF_2, PFF_5, and PFF_10 exhibited response times of 2, 2, and 1.5 s, respectively. These response times were attributed to the incorporation of FeOOH nanoneedles on the PPy surfaces, leading to protuberances and a subsequent increase in the surface area. Therefore, the rapid response occurred because DMMP molecules rapidly diffused into the hybrid PFF nanoparticles due to the high surface area. In contrast, recovery times varied from 3.5 s for the E_PPy to 8.5 s for PFF_10 (PFF_2, 5.5 s; PFF_5, 7.5 s); this effect was attributable to the interaction of the FeOOH nanoneedles with the DMMP gas (Figure 9d). Thus, the E_PPy sensor exhibited about 3 times faster recovery time than the PFF_10 sensor, due to its minimal interaction with the DMMP gas. In addition, increasing PPy nanoparticle diameters decrease sensitivity to DMMP gas because of reducing surface area (Figure S4).

Figure 10a,b presents the electrical response of various PPy nanoparticles upon periodic exposure to 10 ppb of DMMP gas at room temperature. With the exception of pristine PPy, these particles revealed

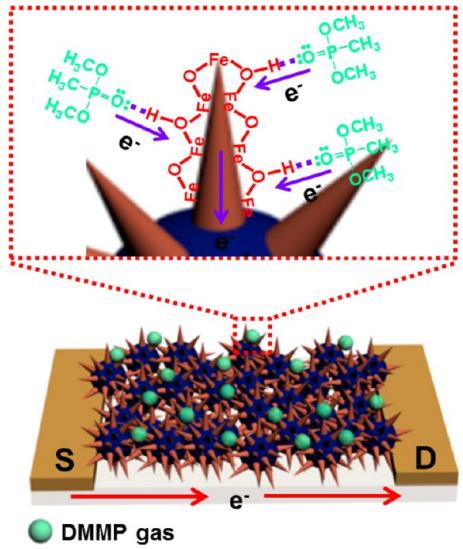

Figure 8. DMMP gas detection mechanism of hybrid PFF nanoparticles at room temperature.

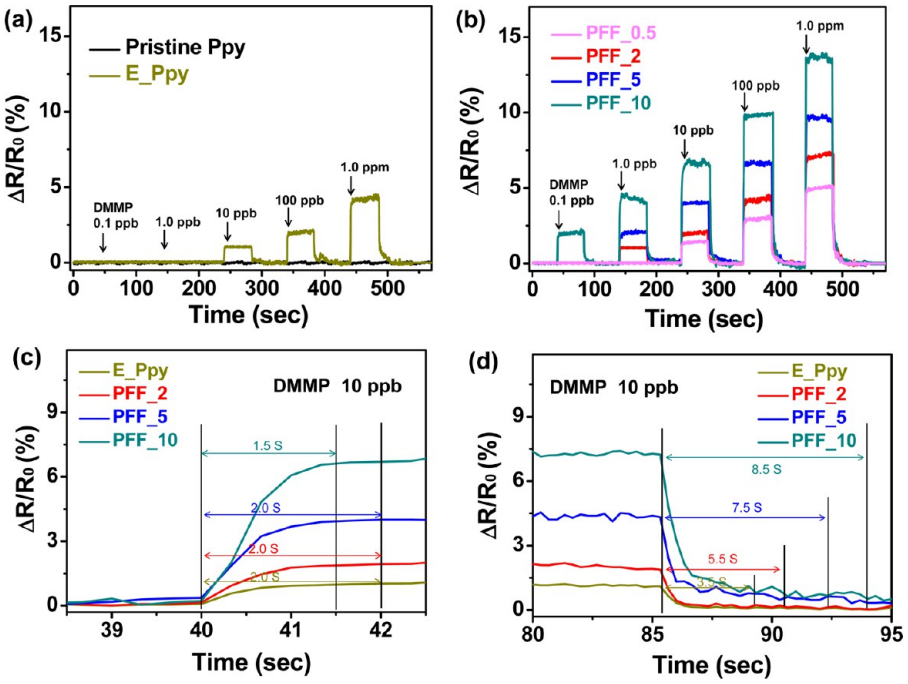

Figure 9. Reversible and reproducible responses are measured at a constant current value (10^{-6} A) with various amounts and types of FeOOH on the PPy surfaces. Normalized resistance changes upon sequential exposure to various DMMP concentrations of (a) pristine (black), E_PPy (yellow), and (b) hybrid PFF nanoparticles (pink, PFF_0.5; red, PFF_2; blue, PFF_5; green, PFF_10). The (c) response and (d) recovery times of hybrid PPy nanoparticles (yellow, E_PPy; red, PFF_2; blue, PFF_5; green, PFF_10) at 10 ppb of DMMP gas at room temperature.

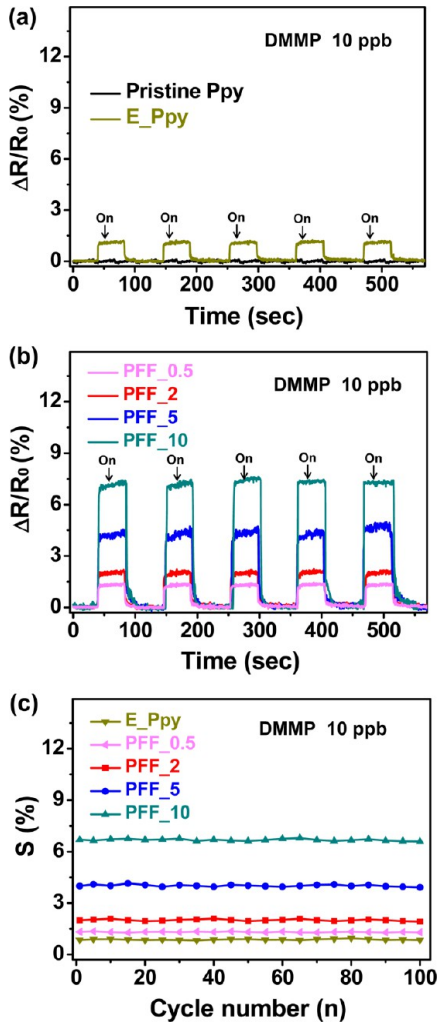

Figure 10. Reversible and reproducible responses are measured at a constant current value (10^{-6} A) with various amount and type of FeOOH on the PPy surfaces. Periodic exposure to DMMP vapor of 10 ppb of (a) pristine (black), E_PPy (yellow), and (b) hybrid PFF nanoparticles (pink, PFF_0.5; red, PFF_2; blue, PFF_5; green, PFF_10). (c) Sensitivity changes of hybrid PFFs nanoparticles with periodic exposure to DMMP vapor of 10 ppb for 100 cylcles (yellow, E_PPy; pink, PFF_0.5; red, PFF_2; blue, PFF_5; green, PFF_10).

similar response sensitivity with enhanced sensing number without retardation of the response or recovery times. Moreover, hybrid PPy nanoparticle gas sensors maintained their sensing ability after 100 cycles (Figure 10c). Furthermore, the morphology of PFFs after DMMP vapor exposure was maintained without collapse of nanoneedles (Figure S5). Figure 11 shows the sensitivity change (*S*) of the sensors as a function of gas concentration; note that the normalized resistance change (sensitivity) should be zero at 0 ppb. At low

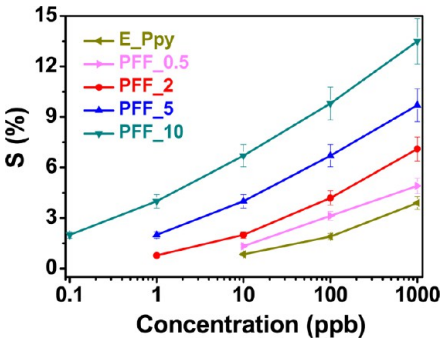

Figure 11. Calibration line of FeOOH decorated PPy particles as a function of DMMP vapor concentration (yellow, E_PPy; pink, PFF_0.5; red, PFF_2; blue, PFF_5; green, PFF_10).

concentrations (<0.1 ppb), the hybrid PFF sensors showed nonlinear changes in sensitivity. Linear behavior was observed over a wide range of concentrations (0.1−1000 ppb). Therefore, the hybrid PFF gas sensors demonstrated reversible, reproducible responses to different analyte concentrations, and their responses were more pronounced as the gas concentration increased. Additionally, these hybrid PFFs can detect other organophosphate nerve gas agents (Figure S6).

CONCLUSION

In summary, we fabricated multidimensional hybrid FeOOH nanoneedle-decorated PPy nanoparticles (PFFs), using a dual-nozzle electrospray technique. To our knowledge, this is the first demonstration of the manufacture of hybrid nanoparticles using the dual-nozzle electrospray method. During the electrospray process, Fe^{3+} ions uniformly dispersed over the PPy surface; compressed air flow through the inner portion of the dual-nozzle prevented particle aggregation. These E_PPy nanoparticles were collected and converted into FeOOH nucleate sites by reacting with OH^- in the NaOH solution in the collector. E_PPy nanoparticles were stirred in an $FeCl_3$ aqueous solution at 70 °C for 4 h to induce growth of FeOOH needles on the surface. The resulting hybrid PFF nanoparticles were used in a gas sensor for the detection of the nerve gas agent, DMMP, with ultrahigh sensitivity at room temperature. Enhanced sensitivity was observed as the size and number density of FeOOH needles on the PPy surface increased. In particular, the PFF_10 sensor transducer exhibited an minimum detectable level (MDL) of 0.1 ppb compared with higher than other hybrid nanomaterial chemical sensors. Thus, this study demonstrated an effective way to fabricate multidimensional organic−inorganic composite hybrid nanomaterials for various electrochemical applications.

MATERIALS AND METHODS

Materials. Poly(vinyl alcohol) (PVA, M_w 9000) and $FeCl_3$ (97%) were purchased from Aldrich Chemical Co. and used without further purification. Pyrrole monomer (98%) and NaOH were also obtained from Aldrich Chemical Co. and used as received.

Fabrication of Hybrid PFF Nanoparticles. Uniformly sized PPy nanoparticles were previously prepared with PVA, $FeCl_3$, and

pyrrole monomer in distilled water, as described in our previous paper.[11] The PPy nanoparticles were mixed with a 10 wt % $FeCl_3$ aqueous solution and then stirred for 4 h at room temperature. The mixed solution was loaded into a syringe pump (KD Scientific, U.S.A.) and then pumped through the outer part of the dual metal nozzle (20 G needle; inner diameter: 0.5 mm). Compressed air flowed through the inner part of the dual-nozzle (27 G needle; inner diameter: 0.1 mm). A voltage of 15 kV was applied between the metal nozzle and the collector Petri dish. The Petri dish collector contained a NaOH aqueous solution to maintain a stable Taylor cone. The distance between the nozzle and collector was 15 cm. The flow rate of the syringe pump was maintained at 0.1 mL h^{-1}. The materials obtained from the electrospray were dispersed in various concentrations of the $FeCl_3$ aqueous solution and stirred for 4 h at 70 °C. The reacted solution was cleaned with ethanol several times and then dried at 60 °C for 12 h.

Characterization of Hybrid PFF Nanoparticles. Transmission electron microscopy (TEM) and high-resolution transmission electron microscopy (HR-TEM) images were obtained with a JEOL JEM-200CX and JEOL JEM-3010 system, respectively. During the sample preparation, the nanomaterials, diluted in ethanol, were cast onto a copper grid. A JEOL 6700 was used to obtain field-emission scanning electron microscopy (FE-SEM) images. X-ray diffraction (XRD) patterns and X-ray photoelectron spectroscopy (XPS) spectra were recorded using the M18XHF SRA (MAC Science Co.) and AXIS-His (KRATOS) systems, respectively. Brunauer–Emmett–Teller (BET) surface areas were measured using a surface area/porosimetry analyzer (ASAP2010, Micromeritics). TGA analysis were recorded on a Pyris6 (Perkin-Elmer). The measurement of the electrical conductivity was carried out at ambient temperature with a source meter, using the four-probe method.

Deposition of Hybrid PPy Nanoparticles on the IDA. The hybrid PFFs (0.5 wt % in ethanol solution) were prepared by ultrasonication for deposition on the as-prepared interdigitated array (IDA). The samples were introduced by a drop-casting method on top of the IDA, to reduce the contact resistance between the particles. The physical adsorption of PFFs on the substrate was followed by drying at room temperature in an inert atmosphere for 1 h to obtain good electrical ohmic contact between the PFFs and electrodes. In the droplet process, a spin-coating method (1000 rpm, 45 s) was used for introducing the uniformly controlled array. A randomly disordered sensor substrate, produced using the drop-casting method, was used as a control.

Electrical Measurement of Sensitivities in Hybrid PFF Sensors. Resistance changes in the hybrid PFF were monitored with a source meter connected to a computer. The hybrid PFF sensors were placed in a vacuum chamber, having a vapor inlet/outlet pressure of 10^0 Torr. Various DMMP gas concentrations (0.1–1000 ppb) were injected into the chamber by a mass flow controller (MFC, KNH Instruments). The real-time resistance was monitored at a constant applied current of 10^{-6} A (defined as $\Delta R/R_0 = (R - R_0)/R_0$, where R and R_0 are the real-time and initial resistances, respectively). After the PFF nanoparticles interacted with various concentrations of DMMP gas for several minutes, each vapor was replaced by compressed air to remove the molecules attached to the backbone of the PFFs. This process was performed repeatedly several times. Vapor/air was supplied at various flow rates of 2–8 slm and 1–5 sccm using the MFC.

Conflict of Interest: The authors declare no competing financial interest.

Supporting Information Available: The contents include the following: (1) SEM and TEM images of pristine PPy nanoparticles; (2) TGA estimate of hybrid PFFs; (3) BET surface area of E_PPy and PFF_0.5 nanoparticles; (4) sensitivity with different diameter of PPy nanoparticles; (5) TEM images of PFF_10 after DMMP exposure; and (6) sensitivity to other organophosphate analytes. This material is available free of charge *via* the Internet at http://pubs.acs.org.

Acknowledgment. This research was supported by the National Research Foundation of Korea (NRF) grant funded by the Korea government (MEST; No. 2011-0017125)

REFERENCES AND NOTES

1. Lee, M. M.; Teuscher, J.; Miyasaka, T.; Murakami, T. N.; Snaith, H. J. Efficient Hybrid Solar Cells Based on Meso-Superstructured Organometal Halide Perovskites. *Science* **2012**, *338*, 643–647.
2. Segar, B.; McCray, J.; Mukherji, A.; Zong, X.; Xing, Z.; Wang, L. An *n*-Type to *p*-Type Switchable Photoelectrode Assembled from Alternating Exfoliated Titania Nanosheets and Polyaniline Layers. *Angew. Chem., Int. Ed.* **2013**, *52*, 6400–6403.
3. Shin, K.-Y.; Hong, J.-Y.; Jang, J. Micropatterning of Graphene Sheets by Inkjet Printing and Its Wideband Dipole-Antenna Application. *Adv. Mater.* **2011**, *23*, 2113–2118.
4. Jang, J.; Ha, J.; Cho, J. Fabrication of Water-Dispersible Polyaniline-Poly(4-styrenesulfonate) Nanoparticles for Inkjet-Printed Chemical-Sensor Applications. *Adv. Mater.* **2007**, *19*, 1772–1775.
5. Wei, Q.; Mukaida, M.; Naitoh, Y.; Ishida, T. Morphological Change and Mobility Enhancement in PEDOT/PSS by Adding Co-Solvents. *Adv. Mater.* **2013**, *25*, 2831–2836.
6. Zhou, C.; Zhang, Y.; Li, Y.; Liu, J. Construction of High-Capacitance 3D CoO@Polypyrrole Nanowire Array Electrode for Aqueous Asymmetric Supercapacitor. *Nano Lett.* **2013**, *13*, 2078–2085.
7. Mai, L.; Dong, F.; Xu, X.; Luo, Y.; An, Q.; Zhao, Y.; Pan, J.; Yang, J. Cucumber-Like V_2O_5/Poly(3,4-ethylenedioxythiophene) and MnO_2 Nanowires with Enhanced Electrochemical Cyclability. *Nano Lett.* **2013**, *13*, 740–745.
8. Patel, S. N.; Javier, A. E.; Beers, K. M.; Pople, J. A.; Ho, V.; Segalman, R. A.; Balsara, N. P. Morphology and Thermodynamic Properties of a Copolymer with an Electronically Conducting Block: Poly(3-ethylhexylthiophene)-*block*-poly(ethylene oxide). *Nano Lett.* **2012**, *12*, 4901–4906.
9. You, J.; Heo, J. S.; Kim, J.; Park, T.; Kim, B.; Kim, H.; Choi, Y.; Kim, H. O.; Kim, E. Noninvasive Photodetachment of Stem Cells on Tunable Conductive Polymer Nano Thin Films: Selective Harvesting and Preserved Differentiation Capacity. *ACS Nano* **2013**, *7*, 4119–4128.
10. Zhai, D.; Liu, E.; Shi, Y.; Pan, L.; Wang, Y.; Li, W.; Zhang, R.; Yu, G. Highly Sensitive Glucose Sensor Based on Pt Nanoparticle/Polyaniline Hydrogel Heterostructures. *ACS Nano* **2013**, *7*, 3540–3546.
11. Song, H. S.; Kwon, O. S.; Lee, S. H.; Park, S. J.; Kim, U.-K.; Jang, J.; Park, T. H. Human Taste Receptor-Functionalized Field Effect Transistor as a Human-Like Nanobioelectronic Tongue. *Nano Lett.* **2013**, *13*, 172–178.
12. Cho, S.; Kwon, O. S.; You, S. A.; Jang, J. Shape-Controlled Polyaniline Chemiresistors for High-Performance DMMP Sensors: Effect of Morphologies and Charge-Transport Properties. *J. Mater. Chem. A* **2013**, *1*, 5679–5688.
13. Kwon, O. S.; Park, S. J.; Lee, J. S.; Park, E.; Kim, T.; Park, H.-W.; You, S. A.; Yoon, H.; Jang, J. Multidimensional Conducting Polymer Nanotubes for Ultrasensitive Chemical Nerve Agent Sensing. *Nano Lett.* **2012**, *12*, 2797–2802.
14. Lee, S. H.; Kwon, O. S.; Song, H. S.; Park, S. J.; Sung, J. H.; Jang, J.; Park, T. H. Mimicking the Human Smell Sensing Mechanism with an Artificial Nose Platform. *Biomaterials* **2012**, *33*, 1722–1729.
15. Yoon, H.; Lee, S. H.; Kwon, O. S.; Song, H. S.; Oh, E. H.; Park, T. H.; Jang, J. Polypyrrole Nanotubes Conjugated with Human Olfactory Receptors: High-Performance Transducers for FET-Type Bioelectronic Noses. *Angew. Chem., Int. Ed.* **2009**, *48*, 2755–2758.
16. Kwon, O. S.; Park, S. J.; Yoon, H.; Jang, J. Highly Sensitive and Selective Chemiresistive Sensors Based on Multidimensional Polypyrrole Nanotubes. *Chem. Commun.* **2012**, *48*, 10526–10528.
17. Choi, S. H.; Ankonina, G.; Youn, D. Y.; Oh, S. G.; Hong, J. M.; Rothschild, A.; Kim, I. D. Hollow ZnO Nanofibers Fabricated Using Electrospun Polymer Templates and Their Electronic Transport Properties. *ACS Nano* **2009**, *3*, 2623–2631.
18. Landau, O.; Rothchild, A.; Zussman, E. Processing-Microstructure-Properties Correlation of Ultrasensitive Gas Sensors Produced by Electrospinning. *Chem. Mater.* **2009**, *21*, 9–11.

19. Kwon, O. S.; Park, S. J.; Park, H.-W.; Kim, T.; Kang, M.; Jang, J.; Yoon, H. Kinetically Controlled Formation of Multidimensional Poly(3,4-ethylenedioxythiophene) Nanostructures in Vapor-Deposition Polymerization. *Chem. Mater.* **2012**, *24*, 4088–4092.
20. Yoon, H.; Jang, J. Conducting-Polymer Nanomaterials for High-Performance Sensor Applications: Issues and Challenges. *Adv. Funct. Mater.* **2009**, *19*, 1567–1576.
21. Yoon, H.; Chang, M.; Jang, J. Formation of 1D Poly(3,4-ethylenedioxythiophene) Nanomaterials in Reverse Microemulsions and Their Application to Chemical Sensors. *Adv. Funct. Mater.* **2007**, *17*, 431–436.
22. Jang, J. Conducting Polymer Nanomaterials and Their Applications. *Adv. Polym. Sci.* **2006**, *199*, 189–259.
23. McQuade, D. T.; Pullen, A. E.; Swager, T. M. Conjugated Polymer-Based Chemical Sensors. *Chem. Rev.* **2000**, *100*, 2537–2574.
24. Jang, J.; Oh, J. H.; Stucky, G. D. Fabrication of Ultrafine Conducting Polymer and Graphite Nanoparticles. *Angew. Chem., Int. Ed.* **2002**, *41*, 4016–4019.
25. Kwon, O. S.; Ahn, S. R.; Park, S. J.; Song, H. S.; Lee, S. H.; Lee, J. S.; Hong, J.-Y.; Lee, J. S.; You, S. A.; Yoon, H.; *et al.* Ultrasensitive and Selective Recognition of Peptide Hormone Using Close-Packed Arrays of hPTHR-Conjugated Polymer Nanoparticles. *ACS Nano* **2012**, *6*, 5549–5558.
26. Kwon, O. S.; Hong, J.-H.; Park, S. J.; Jang, Y.; Jang, J. Resistive Gas Sensors Based on Precisely Size-Controlled Polypyrrole Nanoparticles: Effects of Particle Size and Deposition Method. *J. Phys. Chem. C* **2010**, *114*, 11874–18879.
27. Zhai, D.; Liu, B.; Pan, Y. S.; Wang, Y.; Li, W.; Zhang, R.; Yu, G. Highly Sensitive Glucose Sensor Based on Pt Nanoparticle/Polyaniline Hydrogel Heterostructures. *ACS Nano* **2013**, *7*, 3540–3546.
28. Radhakrishnan, S.; Sumathi, C.; Umar, A.; Kim, S. J.; Wilson, J.; Dharuman, V. Highly Sensitive Glucose Sensor Based on Pt Nanoparticle/Polyaniline Hydrogel Heterostructures. *Biosens. Bioelectron.* **2013**, *47*, 133–140.
29. Xu, M.; Wang, J. Z.; Guo, X.; Xia, H.; Wang, Y.; Zhang, S.; Huang, W.; Wu, S. Gas Sensing Properties of SnO_2 Hollow Spheres/Polythiophene Inorganic−Organic Hybrids. *Sens. Actuators, B* **2010**, *146*, 8–13.
30. Pavlov, V.; Xiao, Y.; Willner, I. Inhibition of the Acetycholine Esterase-Stimulated Growth of Au Nanoparticles: Nanotechnology-Based Sensing of Nerve Gases. *Nano Lett.* **2005**, *5*, 649–653.
31. Royo, S.; Martinez-Manez, R.; Sancenon, F.; Costero, A. M.; Parra, M.; Gil, S. Chromogenic and Fluorogenic Reagents for Chemical Warfare Nerve Agents' Detection. *Chem. Commun.* **2007**, 4839–4847.
32. Dale, T. J.; Rebek, J., Jr. Hydroxy Oximes as Organophosphorus Nerve Agent Sensors. *Angew. Chem., Int. Ed.* **2009**, *48*, 7850–7852.
33. Ji, X.; Zheng, J.; Xu, J.; Rastogi, V. K.; Cheng, T.-C.; DeFrank, J. J.; Leblanc, R. M. (CdSe)ZnS Quantum Dots and Organophosphorus Hydrolase Bioconjugate as Biosensors for Detection of Paraoxon. *J. Phys. Chem. B* **2005**, *109*, 3793–3799.
34. Hratmann-Thompson, C.; Hu, J.; Kaganove, S. N.; Keinath, S. E.; Keeley, D. L.; Dvornic, P. R. Hydrogen-Bond Acidic Hyperbranched Polymers for Surface Acoustic Wave (SAW) Sensors. *Chem. Mater.* **2004**, *16*, 5357–5364.
35. Wang, F.; Gu, H.; Swager, T. M. Carbon Nanotube/Polythiophene Chemiresistive Sensors for Chemical Warfare Agents. *J. Am. Chem. Soc.* **2008**, *130*, 5392–5393.
36. Snow, E. S.; Perkins, F. K.; Houser, E. J.; Badescu, S. C.; Reinecke, T. L. Chemical Detection with a Single-Walled Carbon Nanotube Capacitor. *Science* **2005**, *307*, 1942–1945.
37. Wang, Y.; Hu, N.; Zhou, Z.; Xu, D.; Wang, Z.; Wei, H.; Kong, E. S.-W.; Zhang, Y. Single-Walled Carbon Nanotube/Cobalt Phthalocyanine Derivative Hybrid Material: Preparation, Characterization and Its Gas Sensing Properties. *J. Mater. Chem.* **2011**, *21*, 3779–3787.
38. Raj, V. B.; Singh, H.; Nimal, A. T.; Sharma, M. U.; Gupta, V. Oxide Thin Films (ZnO, TeO_2, SnO_2, and TiO_2) Based Surface Acoustic Wave (SAW) E-Nose for the Detection of Chemical Warfare Agents. *Sens. Actuators, B* **2013**, *178*, 636–647.
39. Hong, J.-H.; Yoon, H.; Jang, J. Kinetic Study of the Formation of Polypyrrole Nanoparticles in Water-Soluble Polymer/Metal Cation Systems: A Light-Scattering Analysis. *Small* **2010**, *6*, 697–686.
40. Xiao, H.-M.; Zhang, W.-D.; Fu, S.-Y. One-Step Synthesis, Electromagnetic and Microwave Absorbing Properties of α-FeOOH/Polypyrrole Nanocomposites. *Compos. Sci. Technol.* **2010**, *70*, 909–915.
41. Tang, B.; Wang, C.; Zhuo, L.; Ge, J.; Cui, L. Facile Route to γ-FeOOH and γ-Fe_2O_3 Nanorods and Magnetic Property of γ-Fe_2O_3 Nanorods. *Inorg. Chem.* **2006**, *45*, 5196–5200.
42. Ho, T. A.; Jun, T.-S.; Kim, Y. S. Material and NH_3-Sensing Properties of Polypyrrole-Coated Tungsten Oxide Nanofibers. *Sens. Actuators, B* **2013**, *185*, 523–529.
43. Park, S. J.; Kwon, O. S.; Jang, J. A High-Performance Hydrogen Gas Sensor Using Ultrathin Polypyrrole-Coated CNT Nanohybrids. *Chem. Commun.* **2013**, *49*, 4673–4675.